PHYSICAL REVIEW B VOLUME 61, NUMBER 1 1 JANUARY 2000-I

Spin-dynamics simulations of the magnetic dynamics of $RbMnF_3$ and direct comparison with experiment

Shan-Ho Tsai,* Alex Bunker,† and D. P. Landau‡
Center for Simulational Physics, The University of Georgia, Athens, Georgia 30602

(Received 12 May 1999)

Spin-dynamics techniques have been used to perform large-scale simulations of the dynamic behavior of the classical Heisenberg antiferromagnet in simple cubic lattices with linear sizes $L \leqslant 60$. This system is widely recognized as an appropriate model for the magnetic properties of $RbMnF_3$. Time evolutions of spin configurations were determined numerically from coupled equations of motion for individual spins using an algorithm implemented by Krech *et al.*, which is based on fourth-order Suzuki-Trotter decompositions of exponential operators. The dynamic structure factor was calculated from the space- and time-displaced spin-spin correlation function. The crossover from hydrodynamic to critical behavior of the dispersion curve and spin-wave half-width was studied as the temperature was increased towards the critical temperature. The dynamic critical exponent was estimated to be $z = (1.43 \pm 0.03)$, which is slightly lower than the dynamic scaling prediction, but in good agreement with a recent experimental value. Direct, quantitative comparisons of both the dispersion curve and the line shapes obtained from our simulations with very recent experimental results for $RbMnF_3$ are presented.

I. INTRODUCTION

Heisenberg models are examples of magnetic systems that have true dynamics with the real time dynamics governed by coupled equations of motion. According to the classification of the different dynamic universality classes proposed by Hohenberg and Halperin in their work on the theory of dynamic critical phenomena,[1] the classical Heisenberg ferromagnet and antiferromagnet are of class J and G, respectively. Although both classes have true dynamics, in the former class the order parameter (the uniform magnetization) is conserved, whereas in the latter the order parameter (the staggered magnetization) is not a conserved quantity. The difference in the dynamic behavior of the Heisenberg ferromagnet and antiferromagnet can already be seen from the linear spin-wave theory, which predicts different low-temperature dispersion curves for the two models. Dynamic critical behavior is describable in terms of a dynamic critical exponent z which depends on conservation laws, lattice dimension, and the static critical exponents. The static critical behavior of three-dimensional Heisenberg models have been studied using a variety of approaches, including a high-resolution Monte Carlo simulation which determined the critical temperature and the static critical exponents for simple cubic and body-centered-cubic lattices.[2] In contrast, the theory of the dynamic behavior of Heisenberg models is not so well understood.

A very close realization of an isotropic three-dimensional Heisenberg antiferromagnet is $RbMnF_3$. Early experimental studies[3–5] have shown that in $RbMnF_3$ the Mn^{2+} ions, with spin $S = 5/2$, form a simple cubic lattice structure with a nearest-neighbor exchange constant of $J^{exp} = (0.58 \pm 0.06)$ meV and a second-neighbor constant of less than 0.04 meV [both defined using our convention for the exchange constant to be shown in Eq. (14)]. Magnetic ordering with antiferromagnetic alignment of spins occurs below 83 K, which we denote as the critical temperature T_c. In this material, the magnetic anisotropy was found to be only about 6×10^{-6} of the exchange field, and no deviation from cubic symmetry was seen at T_c.[6,7] Both the static properties and the dynamic response of $RbMnF_3$ have been examined through neutron-scattering experiments. The early work of Tucciarone *et al.*,[8] found that in the critical region the neutron-scattering function has a central peak (peak at zero frequency transfer) and a spin-wave peak. Later, the experimental study by Cox *et al.*[9] observed a small central peak below T_c as well. The more recent experiments by Coldea *et al.*[10] have also found central peaks for $T \leqslant T_c$, in agreement with previous experiments. From the theoretical side, renormalization-group (RNG) below T_c (Ref. 11) predicts spin-wave peaks, and a central peak in the longitudinal component of the neutron-scattering function. However, at the critical temperature both renormalization-group[12] and mode-coupling[13] theories predict only the spin-wave peak, i.e., the central peak has not been predicted by these theories. The central peak is thought to be due to spin diffusion resulting from nonlinearities in the dynamical equations.[8] In their recent experiment, Coldea *et al.*[10] obtained the most precise experimental estimate of the dynamic critical exponent, $z = (1.43 \pm 0.04)$. The theoretical prediction[1,12,13] is $z = 1.5$ for class G models in three dimensions.

Large-scale computer simulations using spin-dynamics techniques to study the dynamic behavior of Heisenberg ferromagnet and antiferromagnet have been carried out by Chen and Landau[14] and Bunker, Chen, and Landau,[15] respectively. So far, however, there are no direct comparisons of the dispersion curve and the dynamic structure line shapes obtained from simulations with the corresponding experimental results. In the present work we have carried out large-scale simulations of the dynamic behavior of the Heisenberg antiferromagnet on a simple cubic lattice, and make direct comparisons with experimental data for $RbMnF_3$. Section II of

0163-1829/2000/61(1)/333(10)/$15.00

©2000 The American Physical Society

this paper contains the definition of the model and introduces some simulation background. In Sec. III we present and discuss our simulation results and compare them with experiments. Section IV contains some concluding remarks.

II. MODEL AND METHODS

A. Model

The classical Heisenberg antiferromagnetic model is defined by the Hamiltonian

$$\mathcal{H}=J\sum_{\langle \mathbf{r}\mathbf{r}'\rangle}\mathbf{S}_{\mathbf{r}}\cdot\mathbf{S}_{\mathbf{r}'}\,, \tag{1}$$

where $\mathbf{S}_{\mathbf{r}}=(S^x_{\mathbf{r}},S^y_{\mathbf{r}},S^z_{\mathbf{r}})$ is a three-dimensional classical spin of unit length at site $\mathbf{r}$ and $J>0$ is the antiferromagnetic coupling constant between nearest-neighbor pairs of spins. We consider $L\times L\times L$ simple cubic lattices with periodic boundary conditions. The time dependence of each spin can be determined from the integration of the equations of motion [Eq. (2) in Ref. 15], and the dynamic structure factor $S(\mathbf{q},\omega)$ for momentum transfer $\mathbf{q}$ and frequency transfer ω, observable in neutron-scattering experiments, is given by

$$S^k(\mathbf{q},\omega)=\sum_{\mathbf{r},\mathbf{r}'}\exp[i\mathbf{q}\cdot(\mathbf{r}-\mathbf{r}')]\times\int_{-\infty}^{+\infty}\exp(i\omega t)C^k(\mathbf{r}-\mathbf{r}',t)\frac{dt}{\sqrt{2\pi}}, \tag{2}$$

where $C^k(\mathbf{r}-\mathbf{r}',t)$ is the space-displaced, time-displaced spin-spin correlation function defined, with $k=x$, y, or z, as

$$C^k(\mathbf{r}-\mathbf{r}',t)=\langle S^k_{\mathbf{r}}(t)S^k_{\mathbf{r}'}(0)\rangle-\langle S^k_{\mathbf{r}}(t)\rangle\langle S^k_{\mathbf{r}'}(0)\rangle. \tag{3}$$

The displacement $\mathbf{r}$ is in units of the lattice unit cell length a. In the case of antiferromagnets, the wave-vectors are measured with respect to the (π,π,π) point which corresponds to the Brillouin zone center.

B. Simulation method

Using a combination of Monte Carlo and spin-dynamics methods,[14–16] we simulated the behavior of the simple-cubic classical Heisenberg antiferromagnet with $12\leqslant L\leqslant 60$ at the critical temperature $T_c=1.442\,929(77)J^2$ and below T_c. We have chosen units such that the Boltzmann constant $k_B=1$.

Equilibrium configurations were generated using a hybrid Monte Carlo method in which a single hybrid Monte Carlo step consisted of two Metropolis steps and eight overrelaxation steps.[14,15] Typically 1000 hybrid Monte Carlo steps were used to generate each equilibrium configuration and the coupled equations of motion were then integrated numerically, using these states as initial spin configurations. Numerical integrations were performed to a maximum time t_{max}, using a time step of Δt. The space-displaced, time-displaced spin-spin correlation function $C^k(\mathbf{r}-\mathbf{r}',t)$ was computed for time displacements ranging from 0 to t_{cutoff}. Each of such correlations was calculated from an average over between 40 and 80 different time starting points, evenly spaced by $10\Delta t$. Our unit for time is the interaction constant J defined in Eq. (1). The parameters used in this work were as follows. At $T=0.9T_c$ we used lattices sizes $L=12$, 24, 36, 48, and 60, for which the respective time parameters were $(t_{max}J,t_{cutoff}J)=(440{,}400)$, $(440{,}400)$, $(480{,}400)$, $(680{,}600)$, and $(1080{,}1000)$. The respective numbers of initial configurations used were 7020, 2850, 1110, 400, and 810. At T_c and lattice sizes $L=18$, 24, 30, 36, 48 we used $t_{max}J=480$ and $t_{cutoff}J=400$, and for $L=60$ we used $t_{max}J=1080$ and $t_{cutoff}J=1000$. The number of initial configurations used at T_c was 1000 for $L=18{,}30{,}36$, whereas for $L=24$, 48, and 60 the respective numbers were 1125, 715, and 510. Other temperatures considered, chosen to coincide with experimental values, were $T=0.774T_c$, $0.846T_c$, and $0.936T_c$, for which $t_{max}J=480$, $t_{cutoff}J=400$, and the number of initial configurations used was 120. For lattice size $L=24$ at $T=0.9T_c$ the integration was carried out with a time step $\Delta t=0.01J^{-1}$ using a fourth-order predictor-corrector method, as in Refs. 14,15. For other lattice sizes and temperatures, we used a new algorithm[17] based on fourth-order Suzuki-Trotter decompositions of exponential operators, with a time step $\Delta t=0.2J^{-1}$ (except for $L=12$ at $T=0.9T_c$ for which $\Delta t=0.1J^{-1}$). The latter method allowed us to use larger integration time steps and thus to carry out the integration to larger t_{max}, as compared with previous work.[14,15] In the original study of Chen and Landau[14] $t_{max}=120J^{-1}$ and in the work of Bunker *et al.* $t_{max}=200J^{-1}$. In comparison, in the present work we have used a larger $t_{max}\geqslant 440J^{-1}$, more equilibrium initial spin configurations, and a larger lattice size, namely $L=60$. As it is clear from the above, we have concentrated our efforts on two cases: one temperature below T_c, namely $T=0.9T_c$, and at T_c.

We also used the technique of calculating partial spin sums ''on the fly''[14,15] which limits us to data in the $(q,0,0)$, $(q,q,0)$ and (q,q,q) directions with q determined by the periodic boundary conditions,

$$q=\frac{2\pi n}{L},\qquad n=\pm1,\pm2,\ldots,\pm(L-1),L. \tag{4}$$

Since all three Cartesian spatial directions are equivalent by symmetry, the same operation carried out for the $(q,0,0)$ direction was also carried out for the other two reciprocal-lattice directions $(0,q,0)$ and $(0,0,q)$ and the results were averaged. Similarly, the same operations carried out for the $(q,q,0)$ and (q,q,q) directions were also carried out for the equivalent reciprocal-lattice directions and the results were averaged for each case.

For the ferromagnetic case the total magnetization is conserved and the dynamic structure factor $S(\mathbf{q},\omega)$ can be separated into a component along the axis of the total magnetization (longitudinal component) and a transverse component. However, for the antiferromagnet the order parameter is not conserved and separation is not possible. We thus refer to the average

$$S(\mathbf{q},\omega)=\frac{1}{3}[S^x(\mathbf{q},\omega)+S^y(\mathbf{q},\omega)+S^z(\mathbf{q},\omega)] \tag{5}$$

as the dynamic structure factor.

C. Dynamic finite-size scaling

Two practical limitations on spin-dynamics techniques imposed by limited computer resources are the finite lattice size and the finite evolution time. The finite time cutoff can introduce oscillations in $S(\mathbf{q},\omega)$, which can be smoothed out by convoluting the spin-spin correlation function with a resolution function in frequency. The finite-size scaling[14,18] can be used to extract the dynamic critical exponent z using

$$\frac{\omega\overline{S_L^k}(\mathbf{q},\omega)}{\overline{\chi_L^k}(\mathbf{q})}=G(\omega L^z,qL,\delta_\omega L^z) \tag{6}$$

and

$$\overline{\omega_m}=L^{-z}\overline{\Omega}(qL,\delta_\omega L^z), \tag{7}$$

where $\overline{S_L^k}(\mathbf{q},\omega)$ is the dynamic structure factor convoluted with a Gaussian resolution function with characteristic parameter δ_ω, $\overline{\omega_m}$ is a characteristic frequency, defined as

$$\int_{-\overline{\omega_m}}^{\overline{\omega_m}}\overline{S_L^k}(\mathbf{q},\omega)\frac{d\omega}{2\pi}=\frac{1}{2}\overline{\chi_L^k}(\mathbf{q}), \tag{8}$$

and $\overline{\chi_L^k}(\mathbf{q})$ is the total integrated intensity.

For the time cutoffs of at least $400J^{-1}$ used in the present simulations, the oscillations in the dynamic structure factor due to the finite t_{cutoff} were not very significant. Thus we first estimate the dynamic critical exponent z without using a resolution function, or equivalently, we take $\delta_\omega=0$. In this case the analysis is simpler and a value for z can be obtained from the slope of a graph of $\ln(\omega_m)$ vs $\ln(L)$ (where ω_m is the characteristic frequency in the absence of a resolution function) if the value qL is fixed. It is important to note that lattice sizes included in this calculation should be large enough to be in the asymptotic-size regime. The approximate lattice size of the onset of the asymptotic regime can be estimated by looking at the behavior of ωL^z for different lattice sizes using trial values of z.

The effects of the small oscillations in the dynamic structure factor on the dynamic critical exponent z can be evaluated by repeating the analysis using a resolution function. For this purpose, we chose

$$\delta_\omega=0.02\left[\frac{60}{L}\right]^z \tag{9}$$

so that the function $\overline{\Omega}(qL,\delta_\omega L^z)$ in Eq. (7) is a constant if qL is fixed, yielding

$$\overline{\omega_m}\sim L^{-z}. \tag{10}$$

Because δ_ω depends on z, this exponent had to be determined iteratively. We used $n=1,2$ and several initial values for z in the iterations, in order to check the stability of the converged value of z.

III. RESULTS

A. Numerical data for $S(\mathbf{q},\omega)$

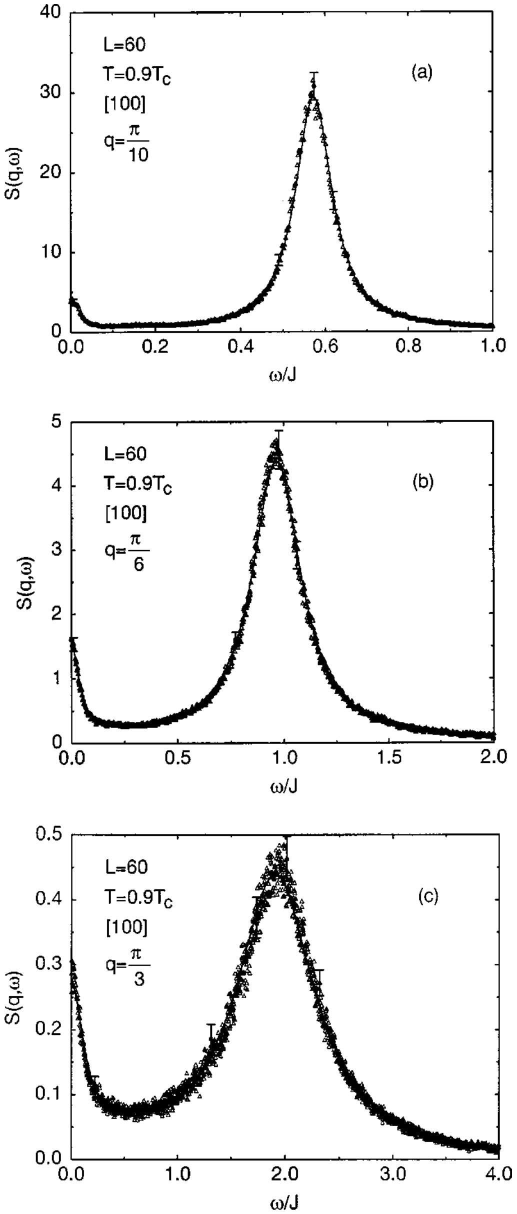

FIG. 1. Dynamic structure factor $S(\mathbf{q},\omega)$ from our simulations for $L=60$ at $T=0.9T_c$ and wave vectors (a) $q=\pi/10$, (b) $\pi/6$, and (c) $\pi/3$ in the [100] direction. The symbols represent spin dynamics data and the solid line is a fit with the Lorentzian function given in Eq. (11). For clarity, error bars are only shown for a few typical points, i.e., error bars for the data in the neighborhood of each of these points are similar. At high frequencies error bars are of the size of the fluctuations in these data.

For $T\leqslant T_c$ our results for the dynamic structure factor, as defined in Eq. (5), show a spin wave and a central peak. In Fig. 1 we show line shapes for lattice size $L=60$ at $T=0.9T_c$ and wave vectors $q=\pi/10$, $\pi/6$, and $\pi/3$ in the [100] direction. We see that as q increases, the central peak broadens and its relative amplitude increases. Figure 2 shows line shapes for $L=60$ at T_c and wave vectors $q=\pi/10$ and $\pi/6$ in the [100] direction. It is clear from these line shapes that the oscillations due to the finite t_{cutoff} are indeed negligible; therefore in our analysis of the line shapes we have not convoluted our results with a resolution function. (As explained in the following section, we later convoluted our results with a Gaussian resolution function in order to directly compare our line shapes with the experiments. The

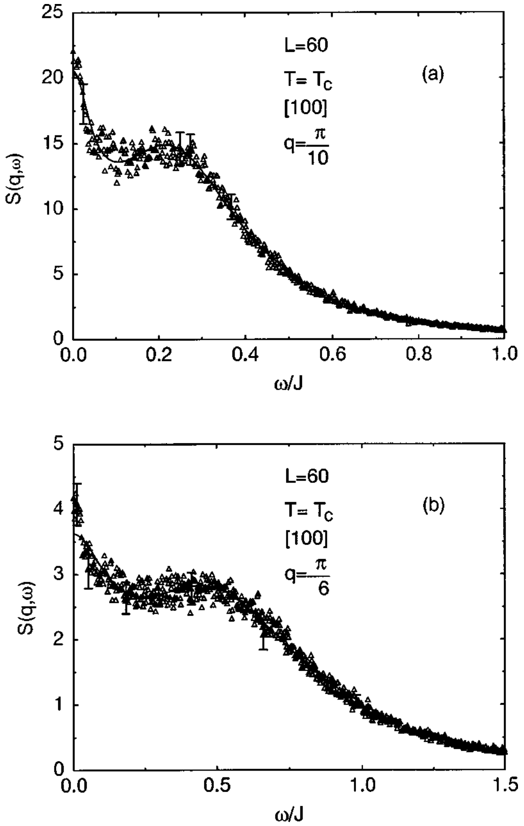

FIG. 2. Dynamic structure factor $S(\mathbf{q},\omega)$ from our simulations for $L=60$ at $T=T_c$ and wave vectors (a) $q=\pi/10$ and (b) $\pi/6$ in the [100] direction. The symbols represent spin dynamics data and the solid line is a fit with the Lorentzian function given in Eq. (11). As in Fig. 1, error bars are only shown for a few typical points.

reason for this is that there is an intrinsic finite resolution in the experimental data due to the finite divergence of neutron beams.) The width of any structure in the line shapes discussed here is much larger than our resolution in frequency $\Delta\omega=1.2\pi/t_{cutoff}$.

Below T_c, previous theoretical[11] and experimental[10] studies motivated us to extract the position and the half-width of the spin wave and central peaks by fitting the line shape to a Lorentzian form

$$S(\mathbf{q},\omega)=\frac{A\Gamma_1^2}{\Gamma_1^2+\omega^2}+\frac{B\Gamma_2^2}{\Gamma_2^2+(\omega+\omega_s)^2}+\frac{B\Gamma_2^2}{\Gamma_2^2+(\omega-\omega_s)^2}, \tag{11}$$

where the first term corresponds to the central peak and the last two terms are contributions from the spin-wave creation and annihilation peaks at $\omega=\pm\omega_s$. For $T=0.9T_c$ we find that Lorentzian line shapes fit our results reasonably well for small values of q, except for the smallest value, namely $q=2\pi/L$, in the [100] direction. The reason is that for each lattice size L, the dynamic structure factor for the smallest value of q corresponds to correlations between spins displaced in space by a distance $L/2$, and the effect of the finite lattice size is particularly prominent in these cases, causing the line shapes to depart significantly from a Lorentzian form. For large values of q [approximately $q>2\pi(L/4-2)/L$] the Lorentzian form given in Eq. (11) does not fit the data, especially at large frequency transfer. In general, the fitted parameters varied when different frequency ranges were used in the fit. Although this variation was small, it was often larger than the statistical error in the fitted parameters obtained from the fit using a single frequency range. Therefore for $T=0.9T_c$ we estimated the error in the fitted parameters by fitting the line shapes using three different ranges of frequency. The values of the parameters were then averaged and the error bars estimated from the fluctuations. At T_c, renormalization-group theory (RNG) (Ref. 12) predicts a non-Lorentzian functional form for the spin-wave line shape, which has been used along with a Lorentzian central peak to analyze experimental data.[10] Since it is more complicated to perform fits to this RNG functional form and since the spin-wave peaks obtained from the simulations are more pronounced than in the experiment, and thus less dependent on the fitted functional, we have fitted the line shapes at T_c to Lorentzians, as given in Eq. (11). Although obtaining a good fit to our data at T_c was more difficult than below T_c, the resulting fits at T_c are still reasonable. Unlike for $T=0.9T_c$, at T_c the line-shape parameters used in the analysis below are the values obtained from the fit to only one frequency range, which was the one that gave the best fit. One should then expect that the actual error in the fitted parameters at T_c is larger (by up to a factor of 5) than the error bars shown in the figures below.

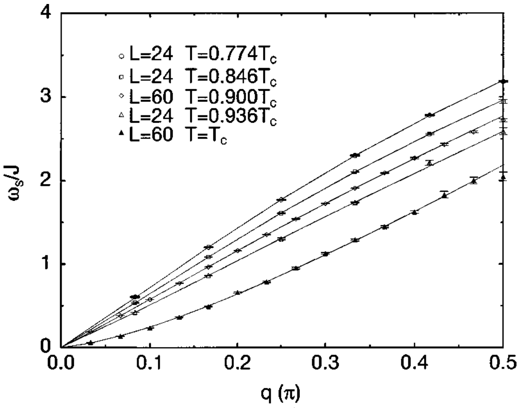

FIG. 3. Spin-wave dispersion relations for $T\leqslant T_c$, in the [100] direction. The symbols represent spin-wave positions extracted from Lorentzian fits to the line shapes from the simulations, and the solid curves are fits of the dispersion relations at different temperatures to Eq. (13).

In addition to the spin-wave and the central peaks, we observed some other peaks on the large frequency tail of the spin-wave peaks. Although these large frequency peaks had very small amplitudes, they could be discerned from the background fluctuations. Using the spin-wave frequencies in the [100], [110], and [111] directions we could check that the position of these extra peaks corresponded to frequencies of two spin-wave addition peaks. These extra structures in the line shapes were particularly visible for the smallest values of wave vectors.

Figure 3 shows how the dispersion curve varies as the temperature increases from $T=0.774T_c$ to T_c. The dispersion curves illustrated here are for the [100] direction and are plotted up to $q=\pi/2$, which corresponds to one half of the Brillouin zone. As mentioned before, for larger values of q the Lorentzian in Eq. (11) did not yield good fits to the line

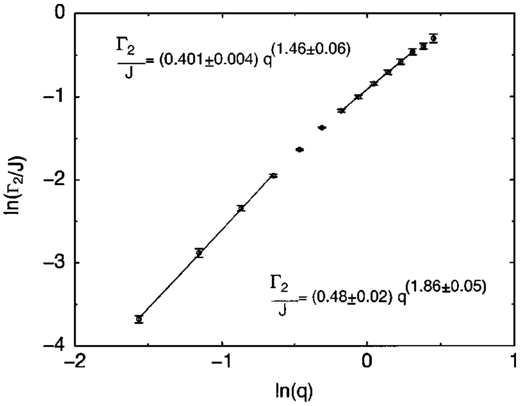

FIG. 4. Log-log graph of the half-width of the spin-wave peak extracted from Lorentzian fits to the line shapes obtained from simulations for $L=60$ and $T=0.9T_c$ in the [100] direction as a function of q.

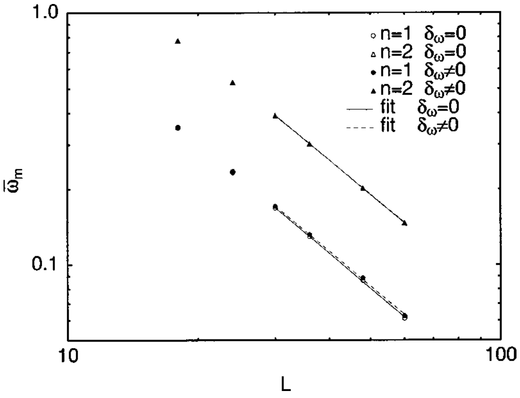

FIG. 5. Finite-size scaling plot for $\overline{\omega_m}$ (with $qL=\text{const}, \delta_\omega L^z = \text{const}$) for the analysis with and without a resolution function. For the former case, the data used correspond to the converged values of z, for $n=1,2$. The error bars were smaller than the symbol sizes.

shapes; however, the spin-wave positions could still be directly read off the graphs, but with larger error bars. For our present purpose of observing the approach to the critical region as the temperature is raised from below T_c, it suffices to consider the dispersion curve for wave vectors up to $q=\pi/2$. Well below T_c, the dispersion relation is linear for small q; as $T \rightarrow T_c$, it changes gradually from linear to a power-law behavior of the form

$$\omega_s = A_s q^x. \tag{12}$$

For $T=0.9T_c$ and $L=60$ a fit including the smallest five q values of the dispersion curve to Eq. (12) yielded $x=1.017 \pm 0.003$. As we probed further away from the Brillouin zone center by including larger values of q in the fit, the exponent decreased slightly. In order to check how sensitive the fitted exponent is to the particular form of the fitted function, we have performed new fits to a function which includes a quadratic term, i.e.,

$$\omega_s = A_s q^x + B_s q^2. \tag{13}$$

Fitting the smallest five q values of the dispersion curve to a function of the form given by Eq. (13) yielded an exponent $x=1.020 \pm 0.003$, which is in good agreement with the value obtained from the previous fit. When larger values of q in the dispersion curve were included in the fits, Eq. (13) tended to yield smaller χ^2's per degree of freedom than Eq. (12). The dispersion curve for $T=T_c$ and $L=60$ fitted to Eq. (12) yielded an exponent of $x=1.38 \pm 0.01$ when the smallest 12 values of q were included in the fit. As the larger q were excluded from the fit, the exponent increased slightly, tending towards $x \simeq 1.40$. When only the smallest few values of q were included in the fit, the exponent decreased again, reflecting the fact that as we probed correlations between spins separated by larger distances (or equivalently, smaller q) the finite size of the lattice (and thus of the correlation length) is revealed, showing that the system is not at criticality. Hence the exponent x decreases towards unity. On the other hand, large values of q correspond to short distance (in the direct lattice space) spin-spin correlations, and the correlation length is much larger than the distance probed. One would thus expect the critical behavior of the system to be manifest, and this is indeed consistent with what we obtained. Our results at T_c are in agreement with the recent experiment[10] which obtained an exponent $x=1.43 \pm 0.04$ when the dispersion curve at T_c was fitted to a power-law relation of the form given in Eq. (12). The solid lines in Fig. 3 are fits to Eq. (13); in general, these fits gave lower values of χ^2 per degree of freedom than fits to Eq. (12).

In the critical region, dynamic scaling theory predicts that the half-width of spin-wave peaks behaves as a power law, $\Gamma_2 \sim q^{1.5}$,[19] whereas for the hydrodynamic regime the prediction from hydrodynamic theory is $\Gamma_2 \sim q^2$.[20] The half-width of the spin-wave peaks at $T=0.9T_c$ and $L=60$ from our simulations is shown in Fig. 4. We observed a crossover from $\Gamma_2=(0.401 \pm 0.004)q^{1.46 \pm 0.06}$ for larger values of wave vector to $\Gamma_2=(0.48 \pm 0.02)q^{1.86 \pm 0.05}$ for small values of q. The behavior for relatively large wave vectors is in agreement with dynamic scaling theory and with the recent experiment.[10] The exponent we obtained by fitting only small values of q is close to the hydrodynamic prediction. Thus for the spin-wave half-width we have observed a crossover of exponents associated with two different regimes, namely, the critical and the hydrodynamic regions. This crossover is similar to the one observed in the dispersion curve at T_c, discussed above. For $T=T_c$ and $L=60$ the spin-wave half-width also had a power-law behavior which varied from approximately $q^{1.2}$ when the 12 smallest values of q were included to approximately $q^{1.4}$ when only the smallest five wave vectors were included in the fit. In their recent experiment, Coldea *et al.*[10] obtained $\Gamma_2 = Dq^{1.41 \pm 0.05}$ for the temperature range $0.77T_c \leqslant T < T_c$, and the coefficient D increased with increasing temperature.

As in the experiments, the dynamic structure factors from our simulations had central peaks (zero frequency transfer peaks) for $T \leqslant T_c$. In contrast, renormalization-group theory predicts a central peak in the longitudinal component of the dynamic structure factor only below T_c,[11] and none of the theories predict a central peak at T_c.[12,13] For $T=0.9T_c$ and $L=60$ fitting the central peak half-width to the form $\Gamma_1 \sim q^x$ yielded very large χ^2 per degree of freedom. A much improved fit was obtained by using the function $\Gamma_1 = A_1 + B_1 q^{C_1}$, which allows for a nonzero central peak width when q vanishes. In these fits the data for the smallest value

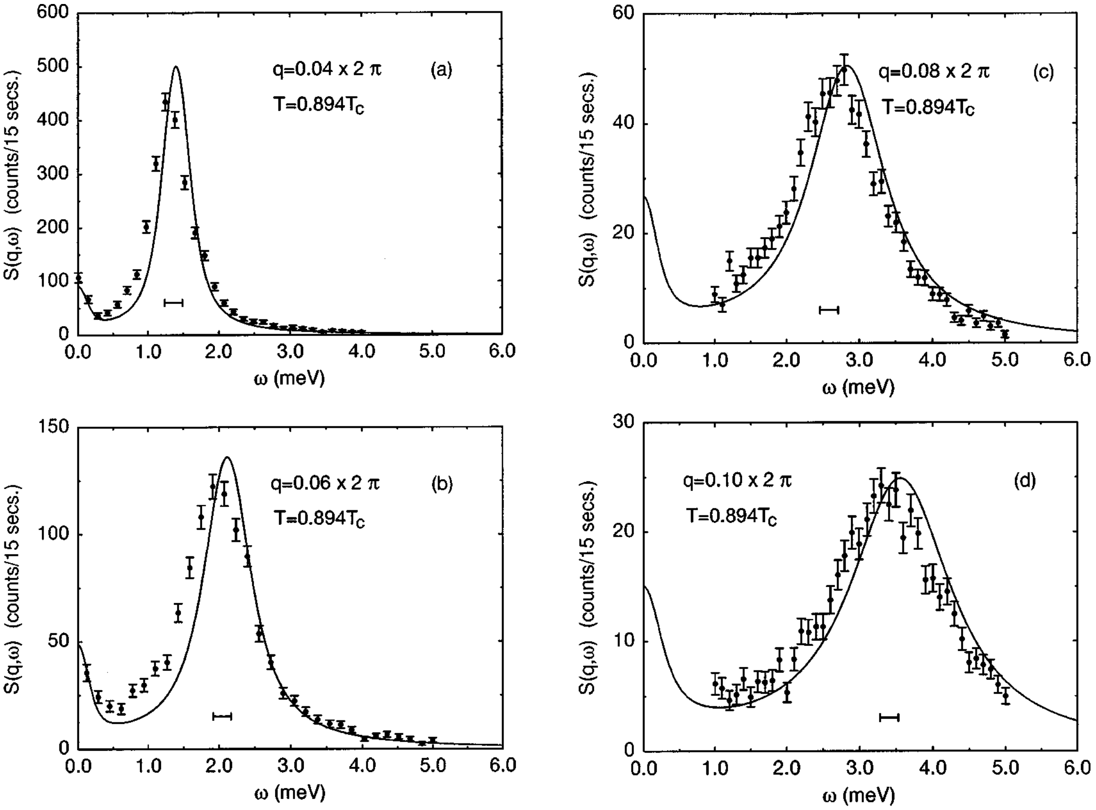

FIG. 6. Comparison of line shapes obtained from fits to simulation data for $L=60$ (solid line) and experiment (open circles) at $T=0.894T_c$ in the [111] direction: (a) $q=2\pi(0.04)$, (b) $q=2\pi(0.06)$, (c) $q=2\pi(0.08)$, and (d) $q=2\pi(0.10)$. The horizontal line segment in each graph represents the resolution in energy (full width at half maximum).

of q observable in $L=60$, i.e., $n=1$, were not included, because of the large finite-size effects in them. The fit including data for q corresponding to $n=2$ until $n=7$ yielded $A_1 \simeq 0.013 \pm 0.001$, $B_1 \simeq 0.120 \pm 0.005$, and $C_1 \simeq 2.4 \pm 0.2$. As we systematically included larger values of q in the fits, these parameters decreased slightly. At T_c we have also fitted the central peaks to Lorentzians, according to Eq. (11); however, these tended to yield curves with smaller amplitudes than the data, as can be seen in Fig. 2. Since there is no theoretical prediction for the central peak, we have also tried to fit them with a Gaussian form. These latter fits were, nevertheless, much worse than the fits with Lorentzians.

The lattice sizes that we used, namely $L=12$, 24, 36, 48, and 60, are all multiples of 12; thus there are certain wave vectors which are common to all lattice sizes. This is an advantage in the study of effects due to finite lattices, because it allows us to compare line shapes and spin-wave dispersion relations for different lattice sizes at a fixed value of wave vector. At $T=0.9T_c$ we did not see a significant finite-size effect for $L \geqslant 24$; however, when we superimposed line shapes at T_c for a fixed value of q, and different values of L, finite-size effects were noticeable for $L=24$. For the larger values of L that we used, the line shapes were the same within the error bars.

The dynamic critical exponent z was extracted from the finite-size scaling of $\overline{\omega}_m$, as described in a previous section. We started the analysis using no resolution function, or equivalently $\delta_\omega=0$, and $n=1,2$. As in previous work,[15] we estimated the lattice $L=30$ to be approximately the onset of the asymptotic-size regime. From the slope of a $\ln(\overline{\omega}_m)$ vs $\ln(L)$ graph fitted with four data points, namely lattice sizes $L=30$, 36, 48, and 60, we obtained $z=1.45 \pm 0.01$ for $n=1$ and $z=1.42 \pm 0.01$ for $n=2$. In order to check the effects of the very small oscillations in $S(\mathbf{q},\omega)$ due to the finite cutoff time, we proceeded to estimate the value of z using a resolution function with δ_ω given by Eq. (9). For the iterations, we used several initial values of $z^{(0)}$, ranging from $z^{(0)}=1.31$ to 1.59, and in all cases the exponent z converged rapidly to the final value with at most three iterations being necessary. For all the initial values of $z^{(0)}$ that we used, we obtained an exponent $z=1.43 \pm 0.01$ for $n=1$ and $z=1.42 \pm 0.01$ for $n=2$. In general, the χ^2 per degree of freedom in the fits for $n=2$ were slightly lower than for $n=1$, although it was reasonable in all cases. Our final estimate for the dynamic critical exponent is $z=1.43 \pm 0.03$, where the error bar reflects the fluctuations in the different estimates of z. A comparison of the characteristic frequency $\overline{\omega}_m$ as a function of the lattice size L for the analysis with and without a resolution function is shown in Fig. 5. For the former case, the graph shown corresponds to the converged values of z for both $n=1$ and 2.

B. Comparison with experiment

In this section we compare our results with the recent neutron-scattering experiment by Coldea *et al.*[10] Before proceeding with the direct comparison, it is necessary to clarify the units and possible normalization factors between simulation and experiment.

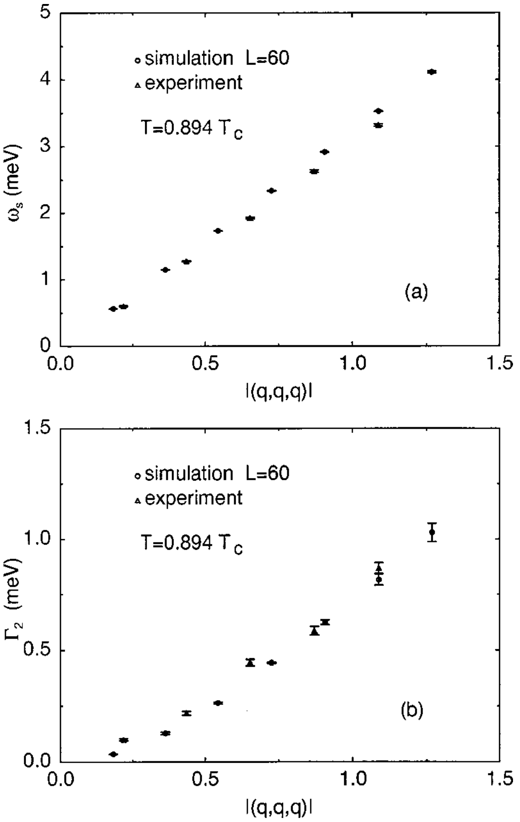

FIG. 7. Comparison of the (a) dispersion curve and the (b) spin-wave half-width, obtained from simulations for $L=60$ (open circle) and the experiment (open triangle) at $T=0.894T_c$, in the [111] direction. The simulation data shown here correspond to values of q accessible with $L=60$, without interpolation to match the q values from the experiment.

The neutron-scattering experiment was done on $\mathrm{RbMnF_3}$, which can be described by a quantum Heisenberg Hamiltonian of the form

$$\mathcal{H}=J^{exp}\sum_{\langle \mathbf{rr}'\rangle}\mathbf{S}_{\mathbf{r}}^{Q}\cdot\mathbf{S}_{\mathbf{r}'}^{Q}, \tag{14}$$

where $\mathbf{S}_{\mathbf{r}}^{Q}$ are spin operators with magnitude $|\mathbf{S}_{\mathbf{r}}^{Q}|^2=S(S+1)$ and the interaction strength between pairs of nearest neighbors was determined experimentally[5] to be $J^{exp}=(0.58\pm0.06)$ meV. In contrast, our simulations were performed on a classical Heisenberg Hamiltonian given in Eq. (1). However, quantum Heisenberg systems with large spin values ($S\geqslant2$) have been shown to behave as classical Heisenberg systems, where the spins are taken to be vectors of magnitude $\sqrt{S(S+1)}$ with the same interaction strength between pairs of nearest neighbors as in the quantum system.[21] In our simulations the spins were taken to be vectors of unit length. Hence to preserve the Hamiltonian the interaction strength J from our simulation has to be normalized according to

$$J=J^{exp}S(S+1). \tag{15}$$

Although this choice of normalization for spin vectors and the interaction strength leaves the Hamiltonian unchanged, it does modify the equations of motions. The dynamics of the classical system so defined is the same as the quantum system defined by the Hamiltonian in Eq. (14) if one rescales the time, or equivalently, the frequency transfer. We obtain

$$\omega^{exp}=J^{exp}\sqrt{S(S+1)}\,\frac{\omega}{J}, \tag{16}$$

where ω^{exp} is the frequency transfer in the quantum system, measured experimentally, and ω/J is the frequency transfer in units of J from our simulations. Parenthetically, we note that the critical temperature of the classical Hamiltonian in Eq. (1) has been determined from simulations to be $T_c=1.442\,929(77)J$.[2] Using the normalization for the interaction strength J given in Eq. (15) and the experimental value[5] $J^{exp}=(6.8\pm0.6)$ K we get $T_c=(85.9\pm7.6)$ K, where the nine percent error comes from the uncertainty in J^{exp}. The experimental value of the critical temperature is around 83 K which is well within the error bars.

Due to detailed balance, neutron-scattering experiments measure the dynamic structure factor multiplied by a temperature and frequency dependent population factor.[10,22,23] This factor does not appear in the simulations of the classical system for which the dynamic structure factor is computed directly. For the comparison, we removed the population factor from the experimental data.

The finite divergence of the neutron beam gives rise to a resolution function which is usually approximated by a Gaussian in the four-dimensional energy and wave-vector space. In the experiment,[10] the measured resolution width along the energy axis was 0.25 meV (full width at half maximum) for incoherent elastic scattering. In order to directly compare our results with the experiment, we convoluted the line shapes from our simulation with a Gaussian resolution function in energy with the experimental value of full width at half maximum, normalized according to Eq. (16). The standard deviation δ_ω thus obtained for the Gaussian resolution function was 0.0619 in units of J. As a test of the effects of the resolution function in the wave-vector space, we have also convoluted our line shapes with a three-dimensional Gaussian function where, for simplicity, we have taken the resolution width in the three wave-vector components to be the same, and equal to the average of the experimental resolution in the longitudinal and transverse directions. The effect of this convolution was found to be negligible; thus the line shapes used in the comparisons shown below do not include the resolution in wave vector.

The experiment[10] performed constant wave-vector scans with both positive and negative energy transfer. The wave-vector transfer $\mathbf{Q}$ was measured along the [111] direction, around the antiferromagnetic zone center which in our notation is the (π,π,π) point. Note that Ref. 10 defines the wave-vector transfer $\mathbf{Q}$ in units such that the antiferromagnetic zone center is (0.5,0.5,0.5); hence to express $\mathbf{Q}$ of Ref. 10 in units of Å^{-1} one has to multiply it by $2\pi/a$, where a is the cubic lattice parameter expressed in Å. However, in the simulation direct lattice positions are defined in units of the lattice constant a; thus we obtain wave vectors multiplied by the constant a. Let us emphasize that one has to divide the wave vector $\mathbf{Q}$ [and also q, see Eq. (4)] defined in this paper by 2π in order to express it in the units used in Ref. 10. In the experiment, measurements were taken for wave vectors $\mathbf{Q}=(\pi+q,\pi+q,\pi+q)$, with $q=2\pi(0.02)$,

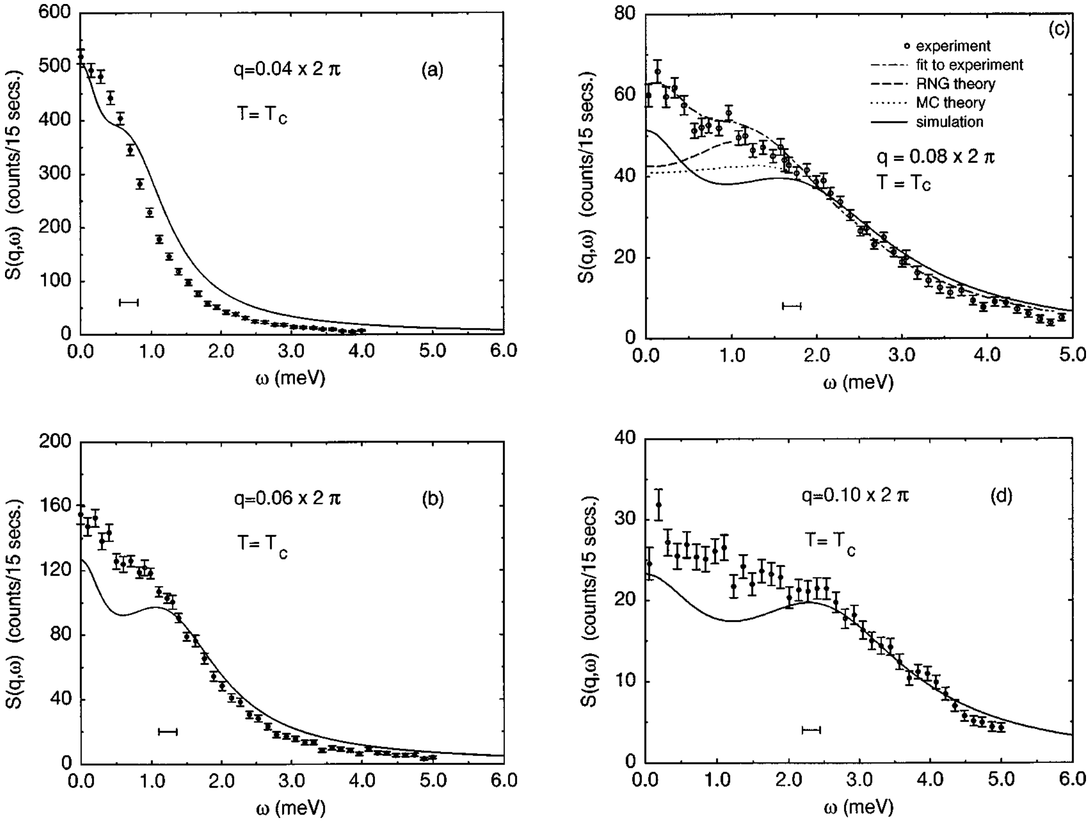

FIG. 8. Comparison of line shapes obtained from fits to simulation data for $L=60$ (solid line) and experiment (open circles) at $T=T_c$ in the [111] direction: (a) $q=2\pi(0.04)$, (b) $q=2\pi(0.06)$, (c) $q=2\pi(0.08)$, and (d) $q=2\pi(0.10)$. The dot-dashed line in (c) is a fit of the experimental data to the functional form predicted by the RNG theory plus a Lorentzian central peak, and the RNG component of the fit is shown by the long-dashed line. The prediction of Mode Coupling (MC) theory for $q=2\pi(0.08)$ is shown by the dotted line in (c). The horizontal line segment in each graph represents the resolution in energy (full width at half maximum).

$2\pi(0.04),\ldots,2\pi(0.12)$, but unfortunately these values of q are not all observed in our simulations with the particular lattice sizes that we used. For instance, with a lattice size $L=60$ we observe wave vectors with $q=2\pi(0.01666\ldots)$, $2\pi(0.03333\ldots)$, ... and so on, according to Eq. (4). Thus in order to directly compare the line shapes from the simulation with the experimental ones, it was necessary to interpolate our results to obtain the same q values of the experiment. This was done by first fitting our line shapes with a Lorentzian form, as given in Eq. (11). Since the parameters B, Γ_2, and ω_s obtained from these fits behave as power laws of q, we linearly interpolated the logarithm of these parameters as a function of the logarithm of q, to obtain new parameters for the line shapes corresponding to those values of q observed in the experiment. We estimated the uncertainties from this procedure to be less than five percent for the parameter B, less than three percent for the spin-wave half-width Γ_2 and the spin-wave position ω_s at T_c, and less than one percent for the spin-wave position ω_s at $T=0.9T_c$. Below T_c, the parameters A and Γ_1 associated with the central peak were linearly interpolated, yielding new parameters with uncertainties of approximately five percent. At T_c, the parameter A was interpolated in the log-log plane (as for B, Γ_2, and ω_s discussed above), whereas Γ_1 was simply linearly interpolated. The uncertainties in A and Γ_1 at T_c were estimated to be less than ten percent. For $L=60$, there is one value of q, namely $q=2\pi(0.10)$, which is accessible to both simulation and experiment. This was the only case for which we did not have to interpolate in q.

Below T_c, the simulations are mainly for $T=0.9T_c$ which unfortunately does not coincide with any temperature used in the experiment; however, it is very close to $T=0.894T_c$ which is one of the temperatures for which experimental re-

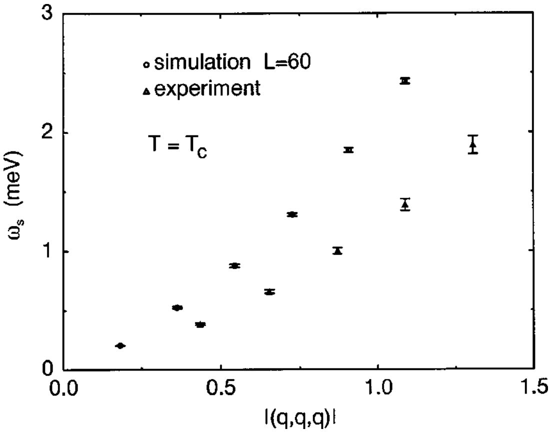

FIG. 9. Comparison of the dispersion curve obtained from our simulation for $L=60$ (open circle) and the experiment (open triangle) at $T=T_c$, in the [111] direction. In the notation here, the first Brillouin zone edge is at $|(q,q,q)|\simeq 2.72$. The simulation data shown here correspond to values of q accessible with $L=60$, without interpolation to match the q values from the experiment.

sults are available. To correct for the slight difference, we made a linear interpolation in temperature, using our results for $L=24$ at $T=0.846T_c$ and at $T=0.9T_c$. We first fitted the line shapes at these two temperatures to a Lorentzian of the form given by Eq. (11), then we linearly interpolated the position and the amplitude of the spin-wave peak at these temperatures, to obtain the spin-wave position and amplitude corresponding to $T=0.894T_c$. For small values of q we found that the frequency of the spin-wave peak at $T=0.894T_c$ was approximately 1.5% larger than at $T=0.9T_c$ and this difference decreased for larger values of q. The spin-wave amplitude at $T=0.894T_c$ was found to be approximately five percent larger than at $T=0.9T_c$ for small values of q. As for the spin-wave position, the difference in the amplitudes decreased for larger values of wave vector.

The intensity of the line shapes in the neutron-scattering experiment was measured in counts per 15 sec. For both temperatures $T=0.894T_c$ and $T=T_c$ the measurements for the several wave vectors were done with the same experimental setup and conditions. Therefore the relative intensities of the line shapes for the different wave vectors is fixed, and equal for both temperatures. The intensity of the line shapes obtained in the simulation had to be normalized to the experimental value; however, because the relative intensities for different wave vectors is fixed, we have only one independent normalization factor for all the wave vectors at both temperatures. The normalization of the intensity was chosen so that the spin-wave peak for $T=0.894T_c$ and $q=2\pi(0.08)$ from the experiment and the simulation matched. This same factor was used to normalize the intensities of the line shapes corresponding to the remaining values of wave vectors at $T=0.894T_c$, and for all cases at T_c. The factor used was 70 counts/15 sec, which we multiplied to the simulated line shapes for all values of q at $T=0.894T_c$ and at T_c.

The final line shapes for $T=0.894T_c$, $L=60$, and several wave vectors are shown in Fig. 6 together with experimental line shapes for each case. Figures 7(a) and (b) show, respectively, the comparisons of the dispersion curve and the spin-wave half-width from the simulation and the experiment at $T=0.894T_c$. The good agreement between our results and experiment can be seen from either the direct comparison of the line shapes, or the comparisons of the dispersion curve and the spin-wave half-width. There is an agreement between the line shape intensities from simulation and experiment over two orders of magnitude, from $q=2\pi(0.02)$ to $q=2\pi(0.10)$. Figure 8 shows the comparison of line shapes from the simulation and the experiment for $T=T_c$, $L=60$, and several values of q. The dispersion curve obtained from the simulations at $T=T_c$, shown in Fig. 9, is systematically larger than the experimental values. We would like to emphasize that the error bars shown for the dispersion curve obtained from our simulations at T_c reflect only the statistical errors of a best fit of the line shapes with Eq. (11). For each wave vector, this fit was done with only one range of frequency; hence errors associated with the choice of frequency range and the quality of the fit were not taken into account. It is reasonable to expect that such sources of error would increase the error bars by a factor of 5. From the direct comparison of the simulated and experimental line shapes at T_c it is difficult to determine the difference in the spin-wave frequencies, because the spin-wave peaks from the experiment are not very pronounced, and their positions have to be extracted from the fits of the line shapes. As we mentioned before, the experimental data at T_c were fitted to a functional form predicted by RNG theory plus a Lorentzian central peak. As an illustration, one such fit is shown in Fig. 8(c) for $q=2\pi(0.08)$, along with the RNG component of the fit and the prediction by mode-coupling theory. Finally, even though at T_c the line-shape intensities from the simulations for small frequency transfer tended to be lower as compared to the experiment, the agreement is still reasonably good, considering the variation of the intensities over almost two orders of magnitude from $q=2\pi(0.02)$ to $q=2\pi(0.12)$.

IV. CONCLUSION

We have studied the dynamic critical properties of the classical Heisenberg antiferromagnet in a simple cubic lattice, using large-scale computer simulations. An interesting time integration technique implemented by Krech *et al.* allowed us to use a larger time integration step and we were thus able to extend the maximum integration time to much larger values than in previous work.

Below T_c, the dispersion curves were approximately linear for wave vectors well within the first Brillouin zone. Increasing the temperature towards the critical temperature the dispersion curve became a power law, reflecting the crossover from hydrodynamic to critical behavior. The power-law behavior of the spin-wave half-width at $T=0.9T_c$ also showed a crossover from critical behavior at large values of q to hydrodynamic behavior at small values of q. The dynamic critical exponent was estimated to be $z=(1.43\pm 0.03)$ which is in agreement with the experimental value of Coldea *et al.*, and slightly lower than the dynamic scaling prediction.

We made direct, quantitative comparison of both the dispersion curve and the line shapes obtained from our simulations with the recent experimental results by Coldea *et al.* At $T=0.894T_c$ the agreement was very good. The major difference was at T_c where spin-wave peaks from our simulations tended to be at slightly larger frequencies than the experimental results. Both at $T=0.894T_c$ and at T_c the line-shape intensities varied over almost two orders of magnitude from $q=2\pi(0.02)$ to $q=2\pi(0.10)$ and there was good agreement between the intensities from simulation and experiment over the whole range. Thus the simple isotropic nearest-neighbor classical Heisenberg model is very good for describing the dynamic behavior of this real magnetic system, except for small differences in spin-wave frequencies at the critical temperature.

ACKNOWLEDGMENTS

We are indebted to Professor R. A. Cowley and Dr. R. Coldea for very helpful discussions and for sending us ascii files of their data. We would also like to thank Dr. M. Krech and Professor H. B. Schüttler for valuable discussions. Computer simulations were carried out on the Cray T90 at the San Diego Supercomputing Center, and on a Silicon Graphics Origin2000 and IBM R6000 machines in the University of Georgia. This research was supported in part by NSF Grant No. DMR-9727714.

[*] Electronic address: tsai@hal.physast.uga.edu

[†] Present address: Max-Planck Institute for Polymer Research, Ackermann Weg 10, Mainz, Germany D-55021-3148. Electronic address: bunker@mpip-mainz.mpg.de

[‡] Electronic address: dlandau@hal.physast.uga.edu

[1] P.C. Hohenberg and B.I. Halperin, Rev. Mod. Phys. **49**, 435 (1977).

[2] K. Chen, A.M. Ferrenberg, and D.P. Landau, Phys. Rev. B **48**, 3249 (1993).

[3] S.J. Pickart, H.A. Alperin, and R. Nathans, J. Phys. (France) **25**, 565 (1964).

[4] D.T. Teaney, V.L. Moruzzi, and B.E. Argyle, J. Appl. Phys. **37**, 1122 (1966).

[5] C.G. Windsor and R.W.H. Stevenson, Proc. Phys. Soc. London **87**, 501 (1966).

[6] D.T. Teaney, M.J. Freiser, and R.W.H. Stevenson, Phys. Rev. Lett. **9**, 212 (1962).

[7] M.J. Freiser, P.E. Seiden, and D.T. Teaney, Phys. Rev. Lett. **10**, 293 (1963).

[8] A. Tucciarone, H.Y. Lau, L.M. Corliss, A. Delapalme, and J.M. Hastings, Phys. Rev. B **4**, 3206 (1971).

[9] U.J. Cox, R.A. Cowley, S. Bates, and L.D. Cussen, J. Phys.: Condens. Matter **1**, 3031 (1989).

[10] R. Coldea, R.A. Cowley, T.G. Perring, D.F. McMorrow, and B. Roessli, Phys. Rev. B **57**, 5281 (1998).

[11] G.F. Mazenko, M.J. Nolan, and R. Freedman, Phys. Rev. B **18**, 2281 (1978).

[12] R. Freedman and G.F. Mazenko, Phys. Rev. Lett. **34**, 1575 (1975); Phys. Rev. B **13**, 4967 (1976).

[13] A. Cuccoli, S.W. Lovesey, and V. Tognetti, J. Phys.: Condens. Matter **6**, 7553 (1994).

[14] K. Chen and D.P. Landau, Phys. Rev. B **49**, 3266 (1994).

[15] A. Bunker, K. Chen, and D.P. Landau, Phys. Rev. B **54**, 9259 (1996).

[16] R.W. Gerling and D.P. Landau, Phys. Rev. B **41**, 7139 (1990).

[17] M. Krech, A. Bunker, and D.P. Landau, Comput. Phys. Commun. **111**, 1 (1998). The second-order Suzuki-Trotter decomposition method has also been implemented by J. Frank, W. Huang, and B. Leimkuhler, J. Comput. Phys. **133**, 160 (1997).

[18] D.C. Rapaport and D.P. Landau, Phys. Rev. E **53**, 4696 (1996).

[19] B.I. Halperin and P.C. Hohenberg, Phys. Rev. Lett. **19**, 700 (1967); Phys. Rev. **177**, 952 (1969).

[20] B.I. Halperin and P.C. Hohenberg, Phys. Rev. **188**, 898 (1969).

[21] See, for example, M.E. Fisher, Rep. Prog. Phys. **30**, 615 (1967); F. Keffer, in *Handbuch der Physik*, edited by H. P. J. Wijn (Springer-Verlag, Heidelberg, 1966), Vol. 18/2.

[22] M. F. Collins, *Magnetic Critical Scattering* (Oxford University Press, New York, 1989).

[23] S. W. Lovesey, *Theory of Neutron Scattering from Condensed Matter* (Clarendon, Oxford, 1984).